Convective variability in real mid-latitude weather

August 21, 2016

1 Introduction

1.1 Motivation

Physical processes which occur on scales smaller than the grid spacing of a numerical model typically have to be parameterized. One such process is convection, which acts to restore stability in the atmosphere and is also the cause of significant amounts of precipitation. Parameterizations represent the effect of these sub-grid scale processes on the resolved scales is represented. Traditionally, this is done in a deterministic way, where the average, most likely, sub-grid effect given a certain large-scale forcing is described. If the sampling size of the unresolved features is large enough, the fluctuations about this mean are indeed small and negligible. So, for example, a grid box of a climate model with several hundreds of kilometers in size contains many convective features, typically 1-10 km in size. Global weather models nowadays, however, have grid spacings on the order of 10 km. Here the sampling size becomes insufficient and the fluctuation about a mean state are significant. Ignoring these fluctuations can lead to systematic biases in the non-linear atmosphere (e.g. Berner et al., 2016) and can also lead to an under-representation of extreme events. Furthermore, in an ensemble system, completely deterministic models are severely underdispersive and, therefore, unreliable.

Stochastic parameterizations aim to solve the problems outlined above. Here, randomness is introduced to represent the variability associated with sub-grid processes. In an ad hoc manner this has been done successfully in medium-range weather prediction for almost two decades (Buizza et al., 1999; Berner et al., 2009). These ad hoc methods, however, are finely tuned to give the appropriate spread-skill relation, and do not actually represent the

1

variability associated with a certain physical process. A more physical way of constructing a stochastic parameterization is to explicitly include a physical model of the uncertainty in the formulation of a parameterization. To get a full representation of the complete model uncertainty this has to be done for every parameterized process individually. One attempt do formulate such a physically-based stochastic parameterization for convection is described now.

1.2 The Craig and Cohen (2006) theory and its application in Plant and Craig (2008)

The (Craig and Cohen, 2006, CC06) theory aims to quantify the mass flux fluctuations of a cloud field in convective equilibrium. Convective equilibrium implies that the average properties of the convection are determined by the large-scale forcing. In more detail, the average total mass flux $\langle M \rangle$ is a function of the large-scales. Other assumptions are: (a) the mean mass flux per cloud $\langle m \rangle$ does not depend on the large-scale forcing, only the mean number of clouds $\langle N \rangle$ does; (b) non-interacting clouds: Cloud are spatially separated (no clustering) and do not influence each other. (c) Equal a priori probabilities: This statistical equilibrium assumption implies that "that clouds are equally likely to occur in any location and with any mass flux". Using these arguments as a basis, a statistical theory is constructed for the distributions of N and m:

$$P(N) = \frac{\langle N \rangle^N}{N!} e^{-\langle N \rangle} \tag{1}$$

$$P(m) = \frac{1}{\langle m \rangle} e^{-m/\langle m \rangle} \tag{2}$$

Combing these, the distribution of the total mass flux M is given by

$$P(M) = \left(\frac{\langle N \rangle}{\langle m \rangle} \right)^{1/2} e^{-\langle N \rangle} M^{-1/2} e^{-M/\langle m \rangle} I_1 \left[2 \left(\frac{\langle N \rangle}{\langle m \rangle} M \right)^{1/2} \right], \tag{3}$$

where $I_1(x)$ is the modified Bessel function of order 1. For large (small) values of $\langle N \rangle$ the shape of this function resembles a Gaussian (Poisson) distribution. It is also possible to derive an equation for the normalized variance of M:

$$\mu_2 = \frac{\langle (\delta M)^2 \rangle}{\langle M \rangle^2} = \frac{2}{\langle N \rangle} \tag{4}$$

Always note that $\langle M \rangle = \langle N \rangle \langle m \rangle$. Eq. 4 can be derived directly from Eq. 3 or from the theory of random sums (Taylor and Karlin, 1998, p.70ff):

Assume $X = \xi_1 + ... + \xi_N$ where ξ_k and N have the finite moments $E[\xi_k] = \mu$, $Var[\xi_k] = \sigma^2$ and $E[N] = \nu$, $Var[N] = \tau^2$. Then the first and second moment of X are $E[X] = \mu\nu$, $Var[X] = \nu\sigma^2 + \mu^2\tau^2$.

The theoretical predictions above were tested against numerical simulations in radiative-convective equilibrium (RCE) by Cohen and Craig (2006). The results of these simulations agreed very well with the theory. The error in μ_2 is around 10%, with $\mu_2\langle N \rangle \approx 1.6$. Other studies introduced time-varying forcings andlooked at the differences in mass flux statistics as described below.

In the (Plant and Craig, 2008, PC08) stochastic parameterization approach, the exponential m distribution (Eq. 2) is used to create a random population of plumes for each grid-box consistent with a large scale $\langle M \rangle$. From this distribution the large-scale tendencies are then computed as the sum of the cloud model output for each plume. $\langle m \rangle = 2 \times 10^7\text{kg s}^{-1}$ is assumed to be a constant. This assumption is motivated by RCE simulations (e.g. Cohen and Craig, 2006). The theoretical prediction for the variance of M (Eq. 4) is not explicitly used in PC08, but comes from the exponential m distribution combined with the random initiation of new clouds. The cloud life time is set to 45 minutes for all clouds.

1.3 Deviations from theory in other studies

Two studies looked at the deviations from the CC06 predictions in their simulations of convection with a time varying forcing: Davies (2008) and Davoudi et al. (2010).

1.3.1 Davies (2008)

She used a model with 1km resolution, a prescribed radiative cooling and time-varying surface fluxes or temperature. For the reference RCE simulation she found $\mu_2\langle N \rangle \approx 1.5$ at 3 km, a deviation of 10% in μ_2, which is in agreement with CC06. When looking at their time-varying simulations, they see that μ_2 is increased (about 2.2) 1h after convection is first triggered and at around 15UTC. They find that at the triggering time and at 18UTC there is strong clustering at scales from 5–20 km.. At the time of maximum convection (12UTC), the RDF is almost uniform and $\mu_2 \approx 0.7$. She argues that the deviation from the predicted variance can be largely explained by clustering.

1.3.2 Davoudi et al. (2010)

They used a similar model setup to CC06, but with a diurnal cycle through interactive radiation, but with a fixed SST. In their Fig. 13, they show their values of $\mu_2\langle N\rangle$ for different heights. They find that for $z <8$ km, this value is less than two. Additionally, in their Fig. 12. they plot histograms of $P(M)$ from their data. They then fit Eq. 3 with $\langle M\rangle$ and $\langle N\rangle$ as free parameters. When they compare these fitted values to the calculated values of $\langle M\rangle$ and $\langle N\rangle$ from their data, they find that $\langle M\rangle$ is similar but the fitted $\langle N\rangle$ is larger than the observed $\langle N\rangle$. They state that "Therefore, predictions of μ_2 are smaller than the corresponding normalized variance from the data. Figure 13 demonstrates that the variance, as well as skewness, is underestimated by the theory close to the cloud base and for the range of altitudes in $z \in [2, 8]$ km."

They then look at two clustering metrics. First, the radial distribution function (their Fig. 14), where they find strong clustering for 5-10 km. Second, $\alpha = \frac{\sigma_N^2}{\langle M\rangle}$, where they find values of about 110% at cloud base, which is in agreement with the findings by CC06 and Davies (2008).

1.4 Research questions

The simple theory of CC06 has been shown to predict the convective variability well in highly idealized simulations and has been used as the basis for the PC08 stochastic convection scheme with some success. Other studies have looked the influence of a time varying forcing and clustering on convective variability, but these studies also used highly idealized setups. So far, there has been no estimate of the convective variability of a "real" weather situation. Particularly the mid-latitudes deviate from RCE simulations in many important ways. The goal of this study is to quantitatively investigate the convective variability in "real" mid-latitude weather and compare the results to the theoretical predictions of CC06. More specifically, the research question is:

RQ1 How does the convective variability of "real" mid-latitude weather situations compare to the predictions of CC06?

Hypothesis There will be some deviations from the theoretical predictions.

If this hypothesis is true, a follow up research questions is:

RQ1.1 Are the deviations from the theoretical prediction similar to what previous idealized studies found? If so, can the change in variability be, to a large extent, explained by clustering?

Hypothesis Clustering can explain most of the deviations from the predicted variance.

If this latest hypothesis is not true, then the next follow up research question is:

RQ1.2 Can other parameters be found to explain the remaining deviations from theory?

Hypothesis External parameters like the convective timescale of orography can explain some of the deviations.

The hope is that by finding these factors in the second hypothesis, stochastic parameterizations can be constructed which include a better representation of the real variability of convection.

2 Methods

2.1 General research strategy

We will use convection-permitting simulations of real weather situations over Germany. A stochastic boundary-layer scheme will be used to create an ensemble where the convection is displaced. We will then use these ensembles to calculate statistics similar to those in CC06 and compare the results to the theoretical prediction. To explain deviations from the theory, we will try to find meaningful measures to characterize the synoptic situation of the case studies and to correlate them with the deviations.

2.2 Numerical experiments

The model used is the COSMO model with 2.8 km horizontal grid spacing Δx and operational COSMO-DE settings with one exception, the stochastic boundary-layer scheme which will be described below. The domain size is 357 grid points in either direction with the domain centered at 10E and 50N. For the analysis a 256 by 256 grid point domain (roughly 717km) at the center of the simulation domain is considered. The 50 grid point gap to the boundary ensures that boundary effects are minimal.

Initial and boundary conditions are taken from the operational COSMO-EU (7km) deterministic forecast with a boundary condition update frequency of 1 h. All runs are started at 00UTC and are run for 24 h. A 20 member ensemble is created by setting a different random number seed in the stochastic boundary-layer scheme for each member. Otherwise, all members are identical, making sure that the large-scale condition are the same and only the convection is shuffled around.

2.2.1 The PSPturb turbulence scheme

The physically-based stochastic perturbation boundary-layer scheme (PSP-turb) is described and tested in (Kober et al., 2016, KC16). A brief outline is given here now.

The PSPbl scheme is additive:

$$\left(\frac{\partial \Phi}{\partial t}\right)_{\text{total}} = \left(\frac{\partial \Phi}{\partial t}\right)_{\text{parameterized}} + \eta \sigma_{\left(\frac{\partial \Phi}{\partial t}\right)_{\text{parameterized}}} \tag{5}$$

These perturbations are process-specific, so for each parameterized process the perturbations have to be calculated separately. The last term in the equation above contains a random number $\eta = N(0,1)$ and the standard deviation of the parameterized tendencies. The random number field has a horizontal correlation length of $5\Delta x$, the effective resolution and is held constant for 10 minutes and then drawn again from scratch. This represents a typical eddy turnover time in the boundary layer. In KC16 the standard deviation term is approximated by

$$\sigma_{\left(\frac{\partial \Phi}{\partial t}\right)_{\text{parameterized}}} = \alpha_{\text{const},\Phi} \frac{l_{\infty}}{5\Delta x} \frac{1}{dt} \sigma_{\Phi}, \tag{6}$$

where $l_{\infty} = 150$ m is the mixing length describing the average size of an eddy. The term σ_{Φ} is the sub-grid scale standard deviation. For the turbulence perturbations the considered variables are vertical velocity w, potential temperature θ and humidity q. The standard deviations are calculated in the turbulence parameterization (see KC06 for details). The factor $\frac{l_{\infty}}{5\Delta x} \propto \frac{1}{\sqrt{N_{\text{eddy}}}}$ scales the variability according to number of unresolved eddies similar to Eq. 4. The factor $\frac{1}{dt}$ converts the term into a tendency term dependent on the time step. Finally, a scaling factor $\alpha_{\text{const},\Phi}$ is included for tuning purposes and should be of order one.

2.3 Case studies

The case studies are all from a recent, convectively active period over Central Europe in May/June 2016 with one exception: We also considered 1 July 2009, which is the test case used in Kober et al. (2016), since this day is a good example of weakly forced diurnal convection.

2.4 Analyses

2.4.1 Identification of clouds and calculation of cloud statistics

To identify clouds, first the fields are converted to binary fields by applying a threshold. Two different fields and thresholds are used for this study: (1) Vertical velocity $w > 1$ m s^{-1} plus a positive cloud water content $q_c > 0$ kg kg^{-1}. The height chosen is 2500 m, which is above the level of shallow convection. The criterion is denoted by the letter m (for mass flux). This criterion was also used by Cohen and Craig (2006) and Davoudi et al. (2010). (2) Instantaneous precipitation rate $pr > 0.001$ mm h^{-1}. This is a surface variable. This criterion is denoted by the letter p.

Contiguous areas are then identified as clouds. Which algorithm??? Optionally, "overlapping" clouds are identified with the local maximum method, followed by a watershed algorithm to find the extent of each separated cloud. If this step is (not) applied, the label ("nowater") "water" is used.

For each identified cloud in each ensemble member a cloud size σ_i is determined as

$$\sigma_i = n_{px}\Delta x^2, \tag{7}$$

where n_{px} is the number of pixels for each cloud i. Furthermore, the mass flux per cloud m_i is computed for criterion (1) as

$$m_i = \Delta x^2 \sum_{px} w\rho, \tag{8}$$

where ρ is density. For criterion (2), the precipitation rate per cloud p_i is calculated as

$$p_i = \sum_{px} pr, \tag{9}$$

Statistics of these variables, such as the mean and the distribution are then calculated (see results).

2.4.2 Calculation of radial distribution functions and clustering parameters

A radial distribution function (RDF) is calculated at each time for each member separately. To do this, the center of mass for each cloud is identified. For these points a two-dimensional pair correlation is computed, where the step size of the search function is $2\Delta x$ and the maximum search radius is $30\Delta x$. The output is normalized, so that a completely randomly distributed field would give an RDF of 1 at all radii. The results are averaged over the ensemble members to give one RDF at each time.

A clustering radius r_c is defined at the point where the RDF drops below 1 (ignoring the first minimum at small radii if present).

2.4.3 Calculation of ensemble means and variances

For the variance calculations, a coarse-graining is applied with edge lengths of 256, 128, 64, 32, 16, 8 and $4\Delta x$. No neighborhoods smaller are considered, since these would be significantly below the effective resolution of the model (Bierdel et al., 2012). For each coarse box, the an average value of m/p is computed, as well as a total mass flux/precipitation rate M/P and the number of clouds N in each box.

To deal with clouds at the boundaries of the coarse-fields, the centers of mass for each cloud is first identified. Then the m_i or p_i is attributed to that one point in space. Therefore, the coarse box which contains the center of mass also contains the entire cloud, while the other box does not contain any of the cloud.

Finally, the variance $\langle(\delta M \mathrm{or} P)^2\rangle$ and the ensemble mean M/P and N are computed for each box and each coarsening scale, resulting in one two-dimensional field for each coarsening scale.

2.4.4 Scatter plots: Comparison with predicted values

To compare the obtained values to the theoretical predictions, the normalized variance for each coarse box j at each coarsening scale n is calculated as

$$\mu_{2j,n} = \frac{\langle(\delta M_{j,n}\mathrm{or}P_{j,n})^2\rangle}{M_{j,n}\mathrm{or}P_{j,n}}. \tag{10}$$

This normalized variance is then plotted against the mean number of clouds $N_{j,n}$. The theory from Eq.4 predicts a slope of 2 for the resulting scatter plot. To get a quantitative comparison of the simulation results and theory, the percent fraction is calculated as

$$\frac{\frac{\mu_{2j,n}}{2}}{M_{j,n}\mathrm{or}P_{j,n}} \times 100\%. \tag{11}$$

2.4.5 Calculation of the convective adjustment timescale

The convective timescale was calculated according to Flack et al. (2016). To produce ensemble mean plots of τ_c the fields are calculated for each ensemble member individually and then averaged. This leads to some not-smooth regions at the edges.

3 Results

3.1 Case 1: 2009070100

3.1.1 Case description

3.2 Cloud statistics

Fig.4 shows histograms of the cloud size σ_i and mass flux m_i or precipitation per cloud p_i alongside the radial distribution function for one time step.

3.3 Variance fields

Fig.4 shows the variance and ensemble mean fields for one time step and one coarsening scale. Blue regions in the bottom left plot indicate less variability compared to theory.

3.4 Variance scatter plots

Fig.4 summarizes the comparison to theory for each coarsening scale.

3.5 Convective adjustment time scale

Fig.4 shows the ensemble mean τ_c. Since the timescale is not always defined for all members, some discontinuities can occur.

3.6 Timeseries plots

Fig.4

References

Berner, J., G. J. Shutts, M. Leutbecher, and T. N. Palmer, 2009: A Spectral Stochastic Kinetic Energy Backscatter Scheme and Its Impact on Flow-Dependent Predictability in the ECMWF Ensemble Prediction System. *Journal of the Atmospheric Sciences*, **66 (3)**, 603–626, doi:10.1175/2008JAS2677.1.

Berner, J., et al., 2016: Stochastic Parameterization: Towards a new view of Weather and Climate Models. *Bull. Am. Meteorol. Soc.*, URL: http://dx.doi.org/10.1175/BAMS-D-15-00268.1.

Bierdel, L., P. Friederichs, and S. Bentzien, 2012: Spatial kinetic energy spectra in the convection-permitting limited-area NWP model COSMO-DE. *Meteorologische Zeitschrift*, **21 (3)**, 245–258, doi:10.1127/0941-2948/2012/0319, URL: http://www.ingentaconnect.com.emedien.ub.uni-muenchen.de/search/article?option1=tka&

Buizza, R., M. Milleer, and T. N. Palmer, 1999: Stochastic representation of model uncertainties in the ECMWF ensemble prediction system. *Quarterly Journal of the Royal Meteorological Society*, **125 (560)**, 2887–2908, doi:10.1002/qj.49712556006, URL: http://doi.wiley.com/10.1002/qj.49712556006.

Cohen, B. G. and G. C. Craig, 2006: Fluctuations in an Equilibrium Convective Ensemble. Part II: Numerical Experiments. *Journal of the Atmospheric Sciences*, **63 (8)**, 2005–2015, doi:10.1175/JAS3710.1, URL: http://journals.ametsoc.org/doi/abs/10.1175/JAS3710.1.

Craig, G. C. and B. G. Cohen, 2006: Fluctuations in an Equilibrium Convective Ensemble. Part I: Theoretical Formulation. *Journal of the Atmospheric Sciences*, **63 (8)**, 1996–2004, doi:10.1175/JAS3709.1, URL: http://journals.ametsoc.org/doi/abs/10.1175/JAS3709.1.

Davies, L., 2008: Self-organisation of convection as a mechanism for memory. Ph.D. thesis.

Davoudi, J., N. A. McFarlane, and T. Birner, 2010: Fluctuation of Mass Flux in a Cloud-Resolving Simulation with Interactive Radiation. *Journal of the Atmospheric Sciences*, **67 (2)**, 400–418, doi:10.1175/2009JAS3215.1, URL: http://journals.ametsoc.org/doi/abs/10.1175/2009JAS3215.1.

Flack, D. L. A., R. S. Plant, S. L. Gray, H. W. Lean, C. Keil, and G. C. Craig, 2016: Characterisation of Convective Regimes over the British Isles. *Quarterly Journal of the Royal Meteorological Society*, n/a–n/a, doi:10.1002/qj.2758, URL: http://doi.wiley.com/10.1002/qj.2758.

Kober, K., G. C. Craig, K. Kober, and G. C. Craig, 2016: Physically Based Stochastic Perturbations (PSP) in the Boundary Layer to Represent Uncertainty in Convective Initiation. *Journal of the Atmospheric Sciences*, **73 (7)**, 2893–2911, doi:10.1175/JAS-D-15-0144.1, URL: http://journals.ametsoc.org/doi/10.1175/JAS-D-15-0144.1.

Plant, R. S. and G. C. Craig, 2008: A Stochastic Parameterization for Deep Convection Based on Equilibrium Statistics. *Journal of the Atmospheric Sciences*, **65 (1)**, 87–105, doi:10.1175/2007JAS2263.1, URL: http://journals.ametsoc.org/doi/abs/10.1175/2007JAS2263.1.

Taylor, H. and S. Karlin, 1998: *An introduction to stochastic modeling.* URL: https://books.google.de/books?hl=en&lr=&id=ppHiBQAAQBAJ&oi=fnd&pg=PP1&dq=An+Introduc
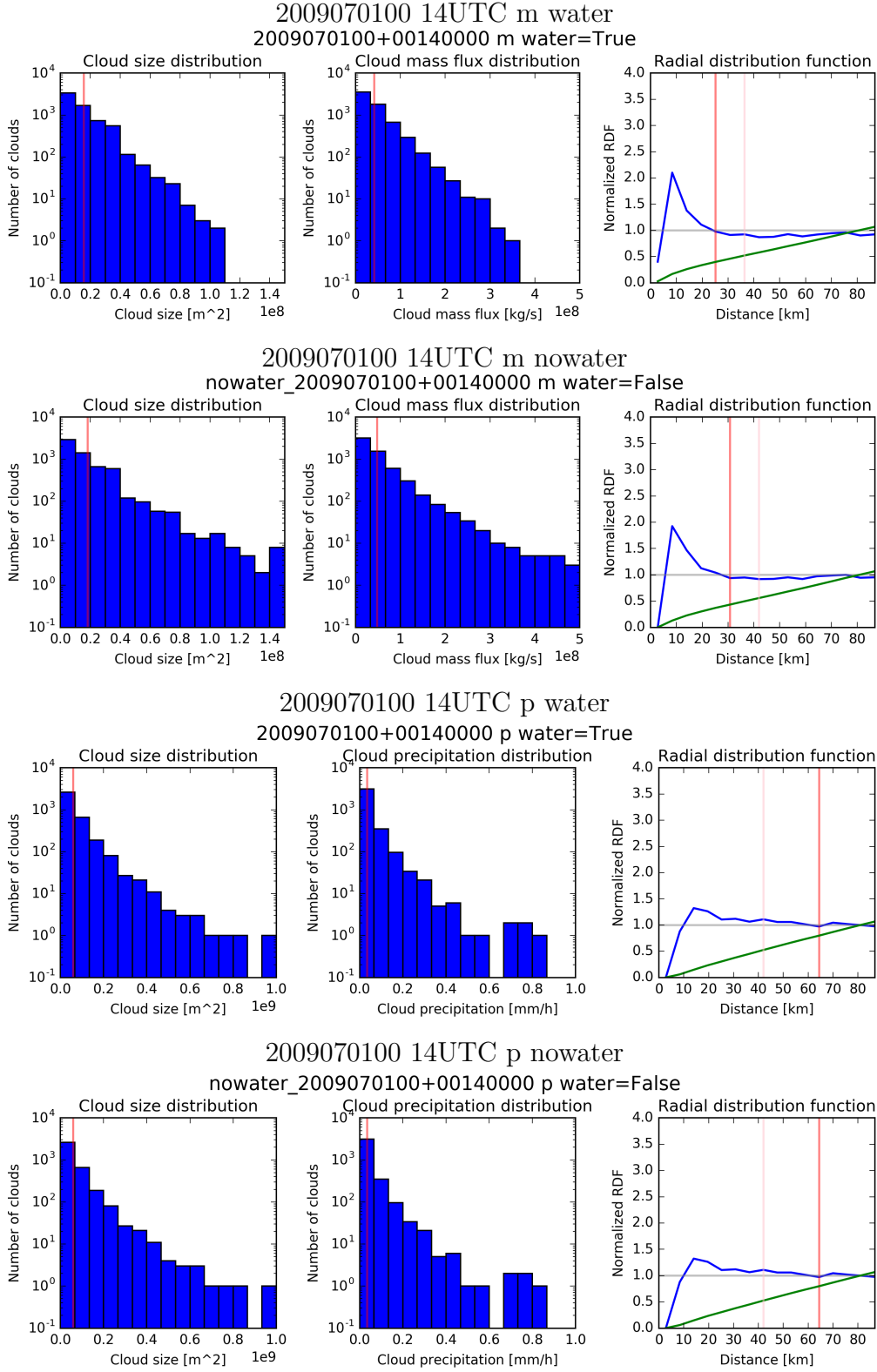
4 Figures

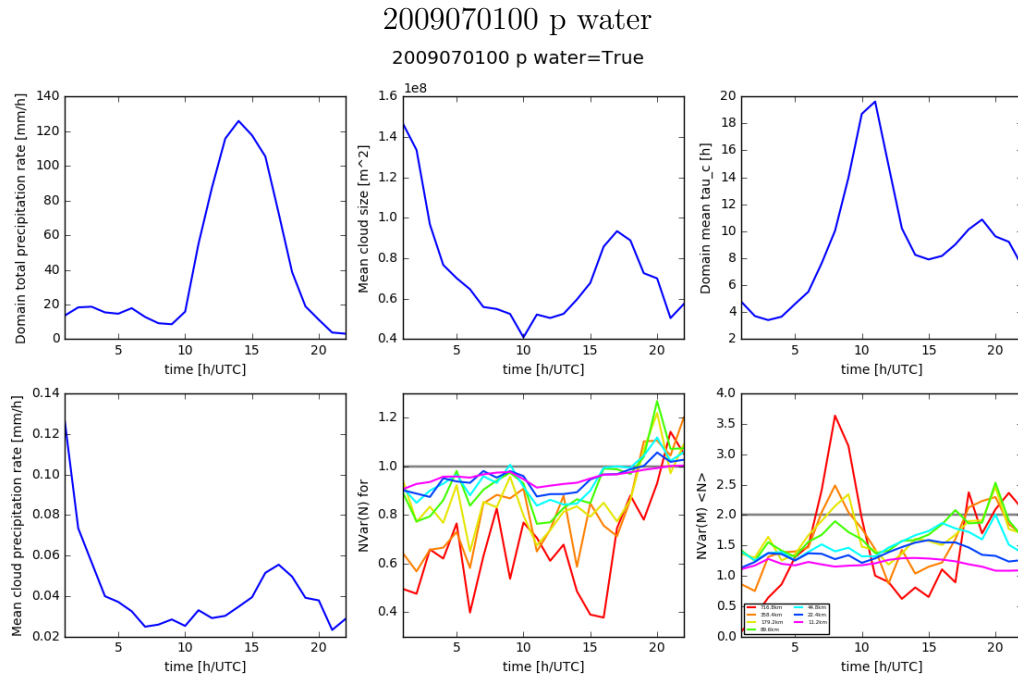Figure 1: Cloud statistics: The left and middle plots are histograms of cloud size (bins = 15 with bin width = 0.1e8/0.67e8) and m_i/p_i(bins = 15 with bin width = 0.33e8/0.067). The red line represents the mean value. On the right plot, the RDF is shown. The red line shows the evaluated clustering radius r_c.
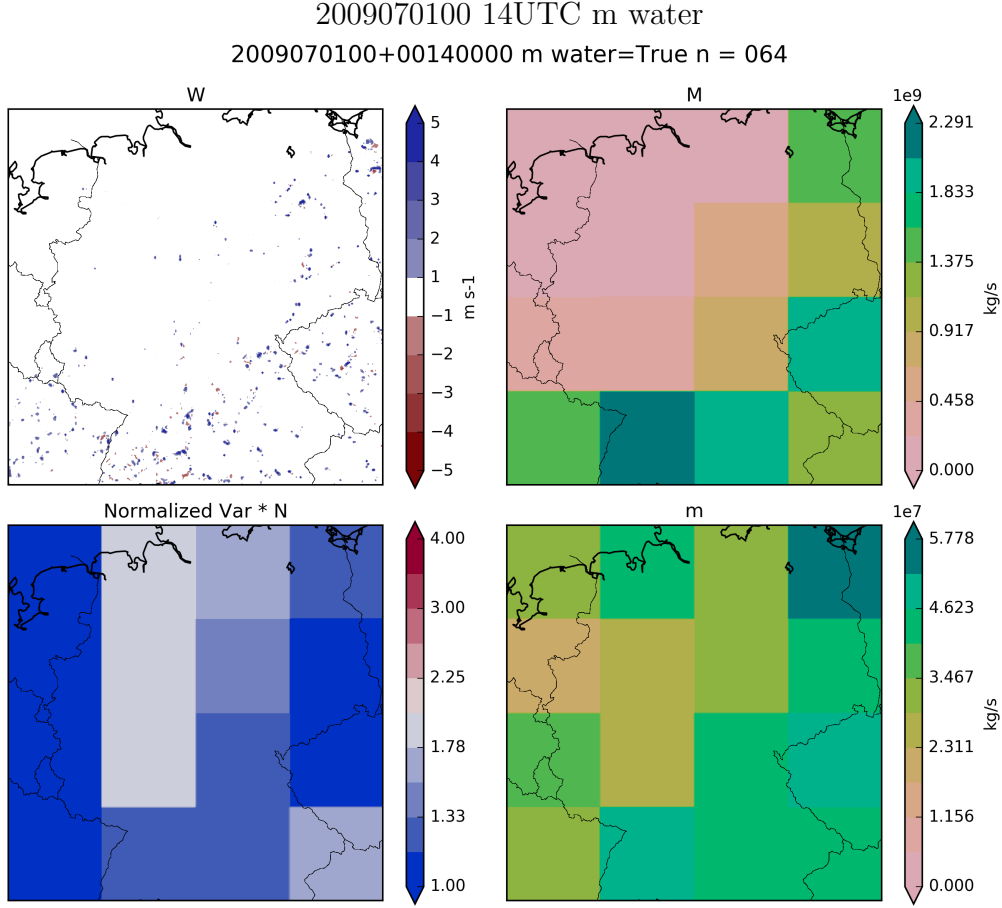
Figure 2: Variance fields: The top left picture shows the vertical velocity field at 2500m height. All blue regions are clouds (given that the cloud water content is positive, not shown). The top right picture shows the ensemble mean total mass flux $M_{j,n}$ for one coarsening scale. The bottom right picture shows the ensemble mean $m_{j,n}$. The bottom right picture shows the Normalized variance divided by the mean cloud number, which the theory predicts to be 2.
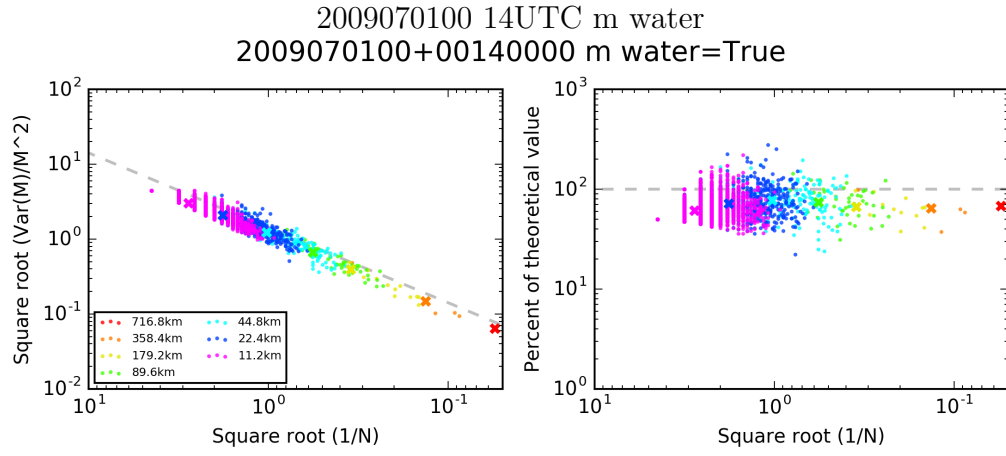
Figure 3: Variance scatter plots: (left) the square root of the normalized variance is plotted against the square root of 1/N. The gray line represents the theoretical prediction. (right) Percentage fraction of theoretical prediction. Crosses represent the mean value for each scale. The mean is calculated in the log-space.

15
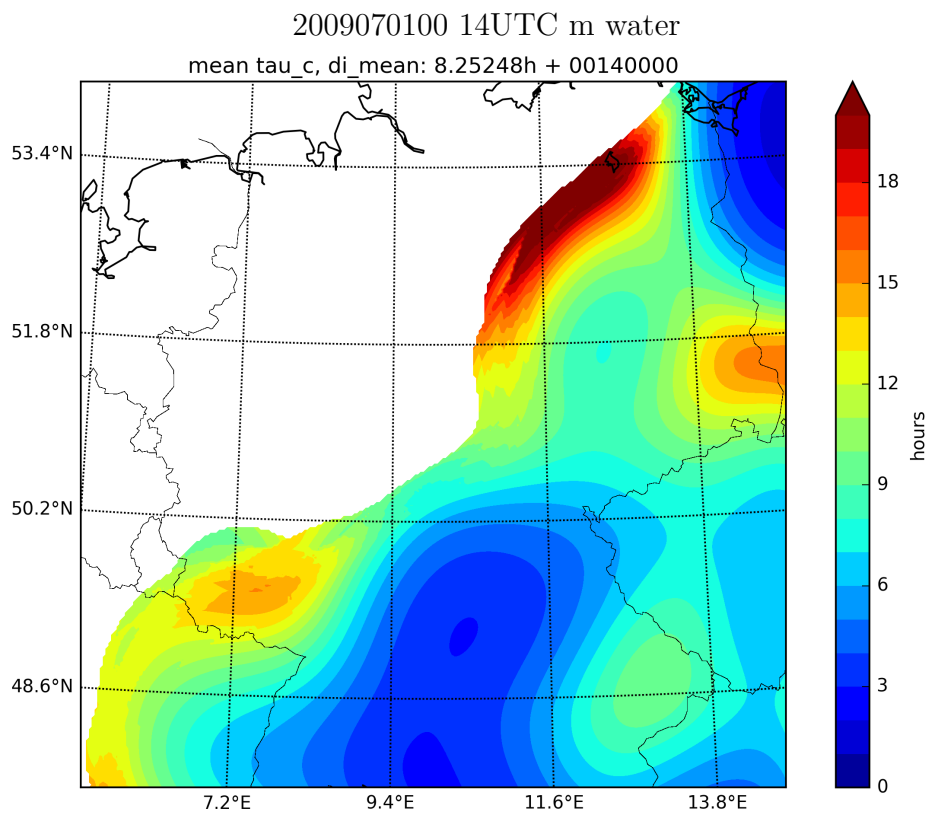
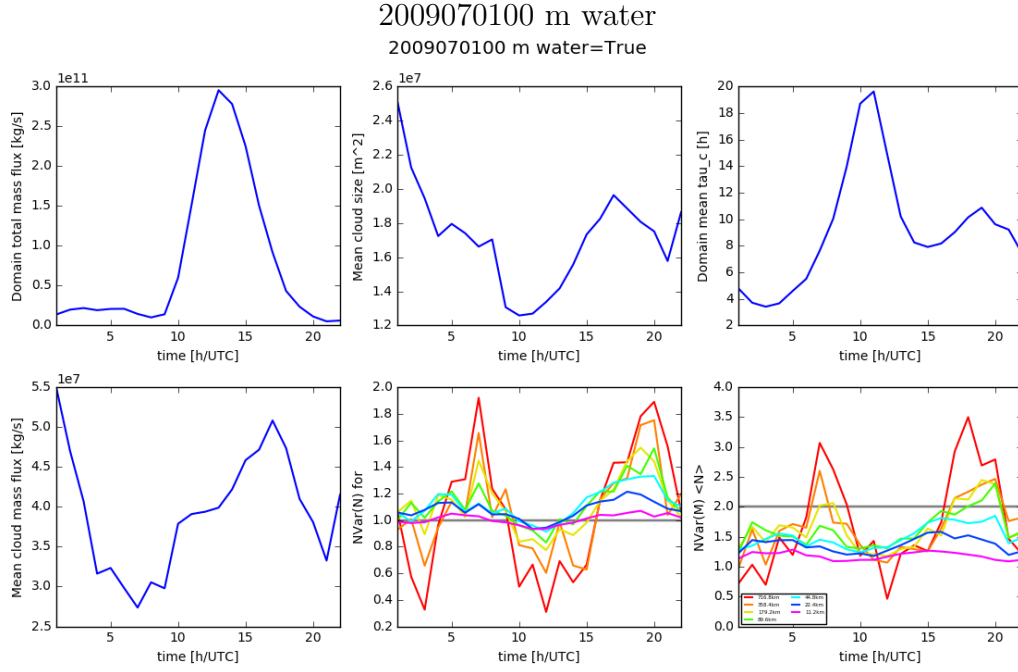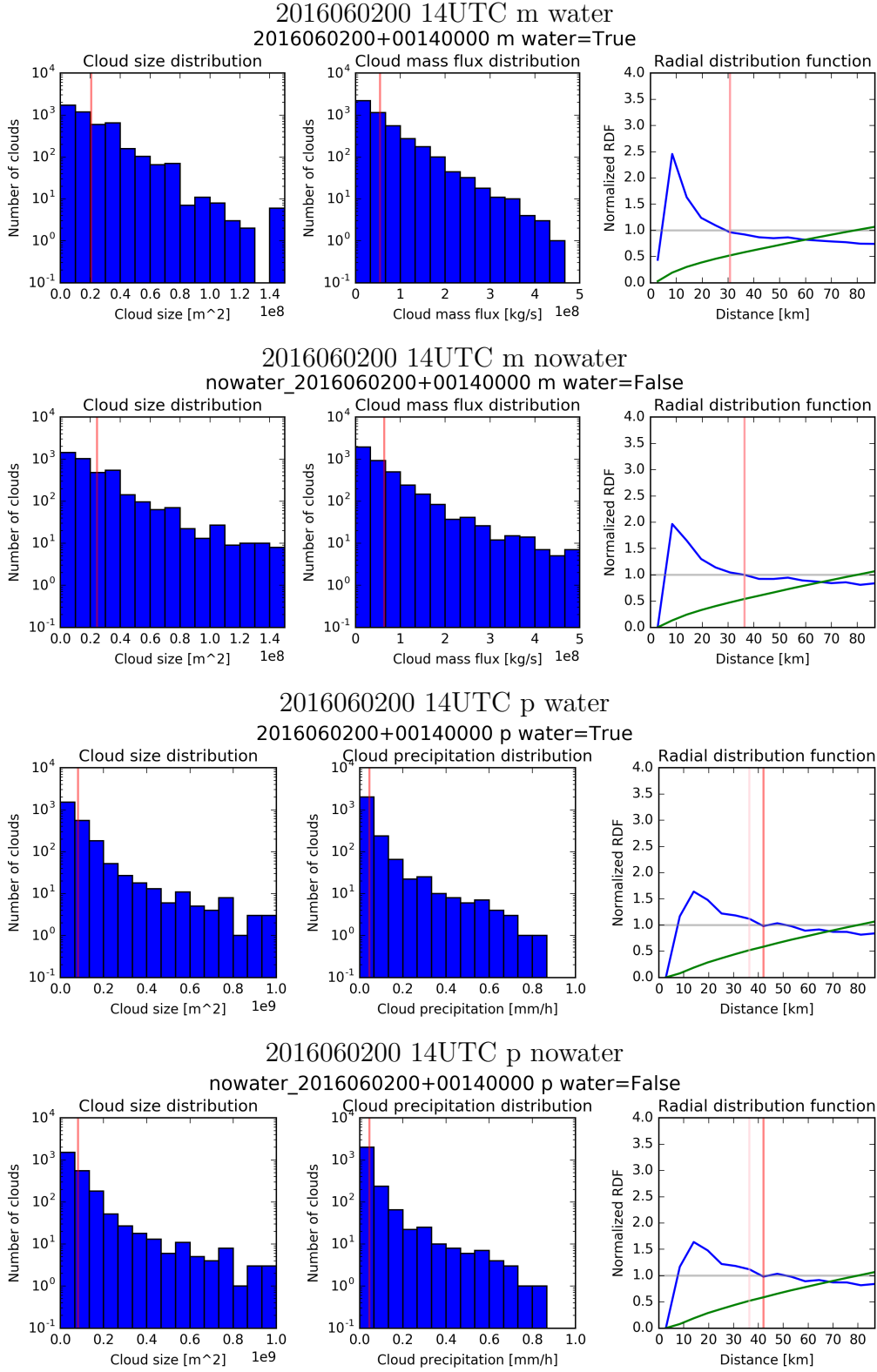Figure 4: Ensemble mean convective adjustment timescale

2009070100 m water

2009070100 m water=True

2009070100 p water

2009070100 p water=True

Figure 5: Timeseries of several values

17

Figure 6: Cloud statistics: The left and middle plots are histograms of cloud size (bins = 15 with bin width = 0.1e8/0.67e8) and m_i/p_i (bins = 15 with bin width = 0.33e8/0.067). The red line represents the mean value. On the right plot, the RDF is shown. The red line shows the evaluated clustering radius r_c.
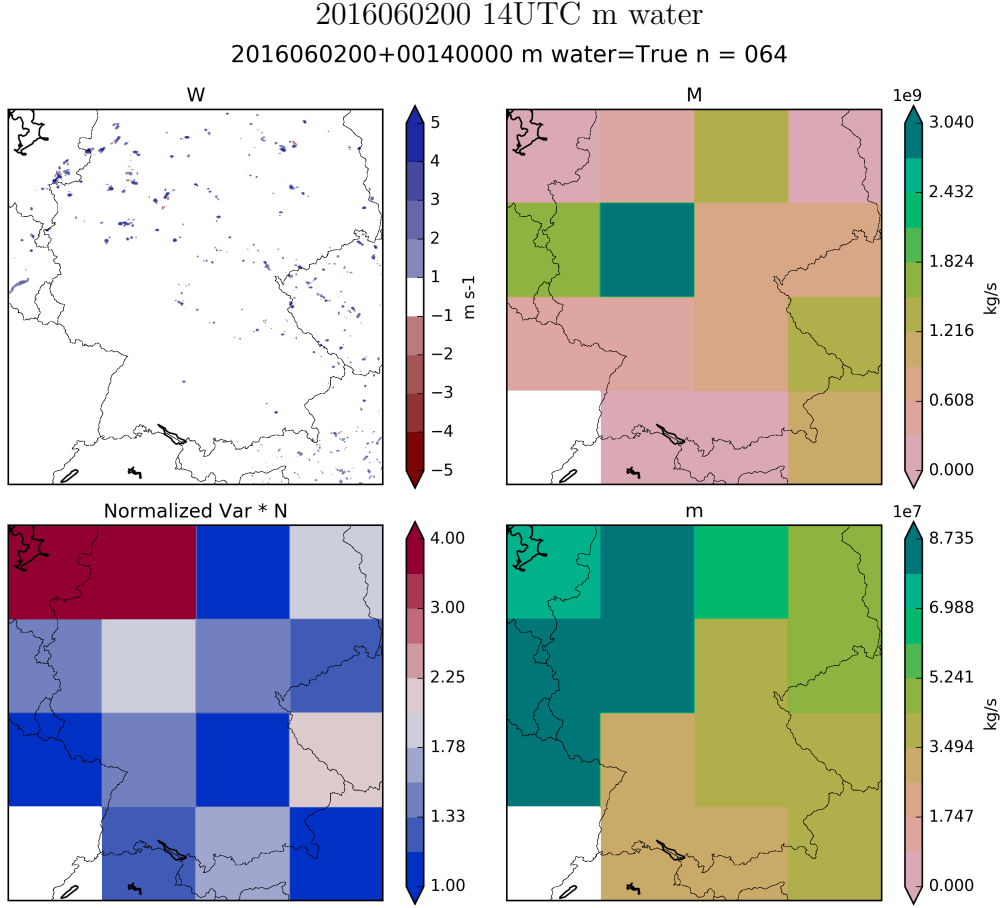
Figure 7: Variance fields: The top left picture shows the vertical velocity field at 2500m height. All blue regions are clouds (given that the cloud water content is positive, not shown). The top right picture shows the ensemble mean total mass flux $M_{j,n}$ for one coarsening scale. The bottom right picture shows the ensemble mean $m_{j,n}$. The bottom right picture shows the Normalized variance divided by the mean cloud number, which the theory predicts to be 2.
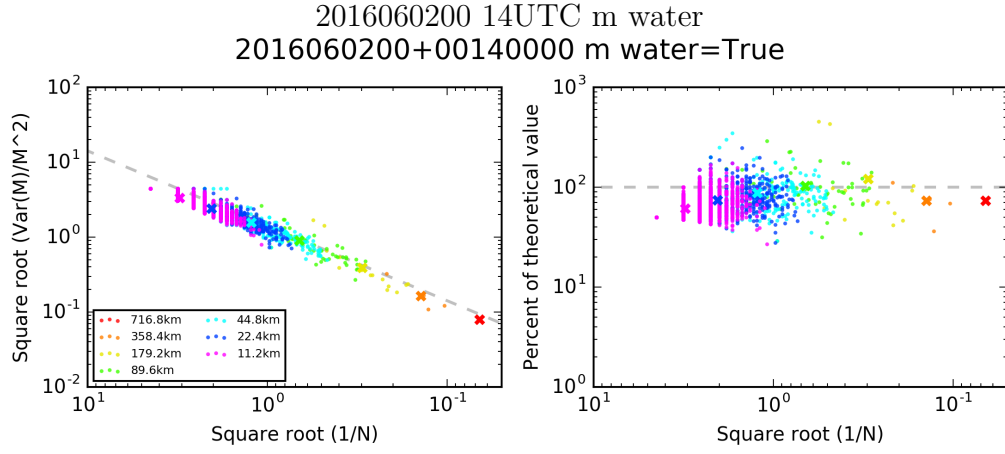
Figure 8: Variance scatter plots: (left) the square root of the normalized variance is plotted against the square root of 1/N. The gray line represents the theoretical prediction. (right) Percentage fraction of theoretical prediction. Crosses represent the mean value for each scale. The mean is calculated in the log-space.
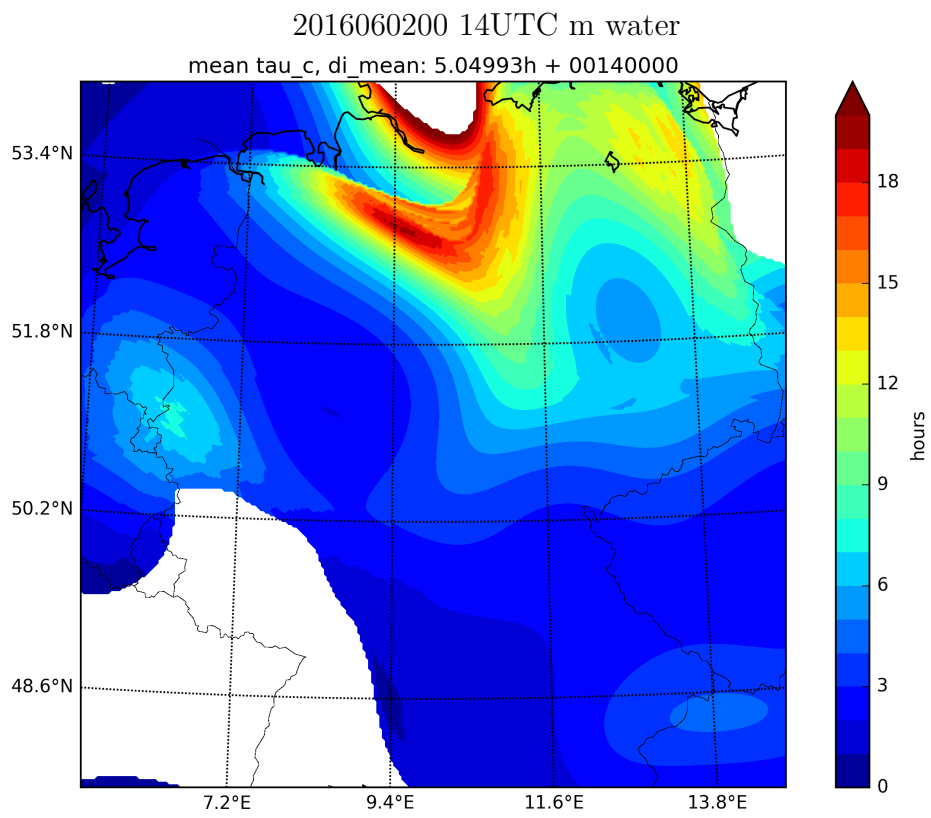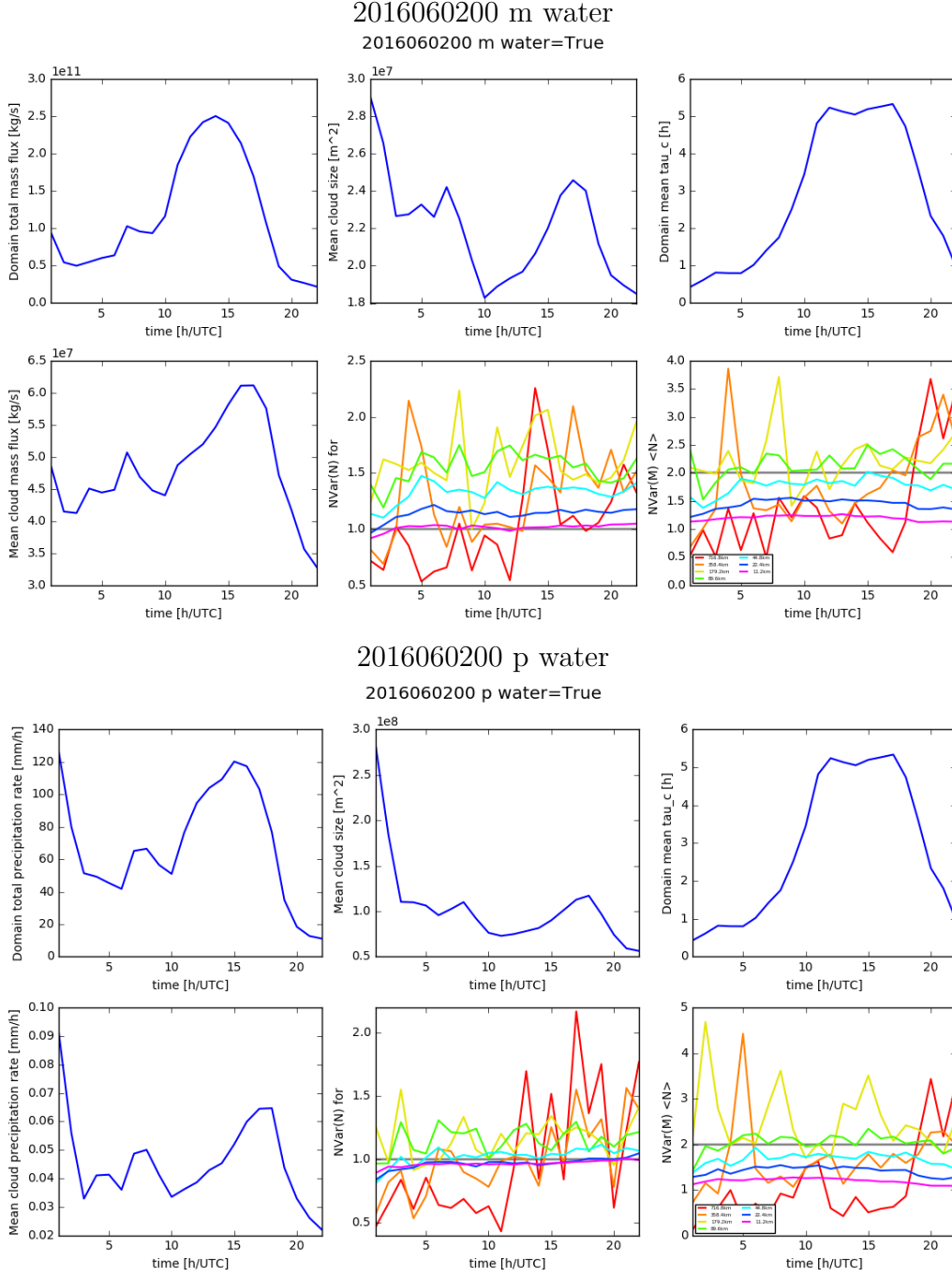
Figure 9: Ensemble mean convective adjustment timescale

Figure 10: Timeseries of several values